



The Pristine survey - XXI: exploring the metal-poor boundary with ESPaDoNS

Linda Lombardo, Piercarlo Bonifacio, Elisabetta Caffau, Patrick François, Pascale Jablonka, Georges Kordopatis, Nicolas Martin, Else Starkenburg, Zhen Yuan, Luca Sbordone, et al.

► To cite this version:

Linda Lombardo, Piercarlo Bonifacio, Elisabetta Caffau, Patrick François, Pascale Jablonka, et al.. The Pristine survey - XXI: exploring the metal-poor boundary with ESPaDoNS. Monthly Notices of the Royal Astronomical Society, 2023, 10.1093/mnras/stad1291 . insu-04093986

HAL Id: insu-04093986




<https://insu.hal.science/insu-04093986>

Submitted on 30 May 2023

HAL is a multi-disciplinary open access archive for the deposit and dissemination of scientific research documents, whether they are published or not. The documents may come from teaching and research institutions in France or abroad, or from public or private research centers.

L'archive ouverte pluridisciplinaire **HAL**, est destinée au dépôt et à la diffusion de documents scientifiques de niveau recherche, publiés ou non, émanant des établissements d'enseignement et de recherche français ou étrangers, des laboratoires publics ou privés.

The Pristine survey – XXI. Exploring the metal-poor boundary with ESPaDoNS

Linda Lombardo ¹★, Piercarlo Bonifacio ¹, Elisabetta Caffau,¹ Patrick François,^{2,3} Pascale Jablonka,^{1,4} Georges Kordopatis,⁵ Nicolas Martin ⁶, Else Starkenburg,⁷ Zhen Yuan ⁶, Luca Sbordone,⁸ Federico Sestito ⁹, Vanessa Hill¹⁰ and Kim Venn ⁹

¹GEPI, Observatoire de Paris, Université PSL, CNRS, 5 place Jules Janssen, F-92195 Meudon, France

²GEPI, Observatoire de Paris, Université PSL, CNRS, 77 Av. Denfert-Rochereau, F-75014 Paris, France

³UPJV, Université de Picardie Jules Verne, 33 rue St Leu, F-80080 Amiens, France

⁴Laboratoire d'Astrophysique, Ecole Polytechnique Fédérale de Lausanne (EPFL), Observatoire de Sauverny, CH-1290 Versoix, Switzerland

⁵Université Côte d'Azur, Observatoire de la Côte d'Azur, CNRS, Laboratoire Lagrange, F-75106 Paris, France

⁶Université de Strasbourg, CNRS, Observatoire astronomique de Strasbourg, UMR 7550, F-67000 Strasbourg, France

⁷Kapteyn Astronomical Institute, University of Groningen, Landjeven 12, NL-9747 AD Groningen, the Netherlands

⁸European Southern Observatory, Alonso de Cordova 3109, Vitacura, Santiago, Chile

⁹Department of Physics and Astronomy, University of Victoria, PO Box 3055, STN CSC, Victoria, BC V8W 3P6, Canada

¹⁰Université Côte d'Azur, Observatoire de la Côte d'Azur, CNRS, Laboratoire Lagrange, Bd de l'Observatoire, CS 34229, F-06304 Nice cedex 4, France

Accepted 2023 April 24. Received 2023 April 17; in original form 2022 November 21

ABSTRACT

In this paper, we study high-resolution spectra of 19 stars that have metallicity estimates below -3.5 using at least two metallicity-sensitive photometric indices based on Pristine photometry. The purpose is to understand what kind of stars populate this parameter space, together with extremely metal-poor stars. This because we plan to extensively use the Pristine photometry to provide extremely metal-poor targets to the WEAVE spectroscopic survey and wish to understand the nature of possible contaminants. We find that this extreme sample of stars is heavily contaminated by variable stars, in particular short period eclipsing binaries. We thus found, serendipitously, eight double-lined spectroscopic eclipsing binaries that could be followed-up in future studies to provide reliable masses and distances for these systems. We also found two stars that have metallicity below -3.0 , one of which may belong to the Gaia-Sausage-Enceladus structure. The lesson to be learned from this investigation is that to select truly metal-poor stars one should be able to remove all photometrically variable stars, which requires complementary information beyond the Pristine photometry. We show how the *Gaia* photometry can be used to remove about 85 per cent of the photometrically variable stars. Our investigation also shows that there is a clear potential for Pristine photometry to find double-lined spectroscopic binaries among short period eclipsing binaries.

Key words: stars: abundances – stars: Population II.

1 INTRODUCTION

The Pristine survey (Starkenburg et al. 2017) is observing the Northern hemisphere using the MegaCam wide-field imager (Boulade et al. 2003) on the Canada–France–Hawaii Telescope (CFHT) at Mauna Kea, with a narrow-band filter centred on the Ca II H&K lines in the near UV. This narrow-band filter, combined with Sloan Digital Sky Survey (SDSS) *gri* filters (Doi et al. 2010) has been proven to provide reliable metallicity estimates and to be an excellent tool to find metal-poor stars. In the last 6 yr, we have conducted spectroscopic follow-up observations with various facilities both to improve the calibration of the Pristine photometric metallicity and to study in depth some of the most metal-poor stars that can be found. A major highlight has certainly been the discovery and detailed study of star Pristine.221.8781 + 9.7844 (Starkenburg et al. 2018; Lardo et al. 2021). This star with $[\text{Fe}/\text{H}] = -4.79$ is one of the dozen of

stars with $[\text{Fe}/\text{H}] \leq -4.5$ and one of the only two that is not clearly carbon-enhanced, casting some doubts on the claims that at very low $[\text{Fe}/\text{H}]$ all stars must be carbon enhanced (e.g. Frebel, Johnson & Bromm 2007). Another quite exceptional star discovered thanks to the Pristine Survey is Pristine.237.8588 + 12.5660 (Aguado et al. 2019; Kieft et al. 2021; Lardo et al. 2021). With $[\text{Fe}/\text{H}] = -4.22$, this star is among the most metal-poor objects known. Both these stars are in the sub-giant stage and, according to standard stellar evolution theory, their Li content should be the same as at their formation, yet both have a measurable Li, but well below the constant value observed in stars in the metallicity range -4.0 to -1.5 and called the Spite Plateau (Spite & Spite 1982a,b). They are part of what is usually referred to as the Spite Plateau ‘meltdown’ (Sbordone et al. 2010). In Bonifacio et al. (2019) we demonstrated the added value that is provided to the Pristine metallicity calibration, by including also the information provided by the parallax. This sophisticated analysis, which combines *Gaia* parallaxes, photometry (Gaia Collaboration et al. 2016) and Pristine photometry, allowed us to select a very interesting sample of metal-poor stars, which we observed with

* E-mail: linda.lombardo@obspm.fr

FORS2 at the ESO 8.2 m telescope, including a sizeable number of stars with low α/Fe ratios. Such stars could have been formed in dwarfs galaxies with a low, or bursting, star formation and then accreted by the Milky Way (Caffau et al. 2020). The CFHT, in spite of its medium size, proved to be very effective in performing such follow-up observations with the ESPaDOnS spectrograph (Venn et al. 2020; Lucchesi et al. 2022). For this reason, we decided to boldly target a sample of stars with estimated $[\text{Fe}/\text{H}] < -3.5$, disregarding any complementary information. The purpose was to see what kind of stars we would find and to explore the limitations of a selection based on Pristine and SDSS photometry alone. The purpose of this is to help us to use Pristine photometry to select metal-poor stars for the spectroscopic survey to be conducted in the next five years with the multi-object facility WEAVE (Jin et al. 2023) on the William Herschel 4.2 m telescope.

We did expect several kinds of contaminants, that is, stars that are not as metal poor as predicted by the Pristine photometry. Among these we expected young, chromospherically active stars, with emission in the cores of the Ca II H&K lines. All kinds of variable stars (RR Lyrae are typically found in the colour range investigated by us) are also expected to be contaminants, since the SDSS broad-band photometry was taken at a different time with respect to the Pristine photometry, which leads to combining photometric bands that are observed at different phases in the light curve. What we did not expect was to find a majority of short-period eclipsing binaries, as discussed in Section 4, and especially double-lined spectroscopic binary (SB2) stars. With hindsight, a percentage of such contaminants should have been expected. One of the characteristics of short period binaries is the tidal locking, which leads to a synchronisation of orbital and rotational velocities. In turn, this results in larger rotational velocities than found in non-double stars of the same spectral type. These high rotational velocities imply that the Ca II H&K lines are shallow and their narrow-band photometry mimics a low metallicity. This effect comes on top of the above-mentioned photometric variability.

2 TARGET SELECTION

The 19 stars in the sample were selected from the Pristine catalogue with the request that both metallicity based on *CaHK* narrow band and both $g - i$ and $g - r$ broad-band colours were below -3.5 . Complementary requests were also the observability in α in the CFHT period 20B and $g < 15.5$. In Fig. 1, we show the positions of our targets in the usual colour-colour plot used by the Pristine collaboration, coloured with their metallicity estimate derived from the Pristine *CaHK* and $g - i$, compared with theoretical colours for two different surface gravities and metallicities. The most commonly used version of this plot is shown in fig. 3 of Starkenburg et al. (2017), where the solid lines represent exponential fits to theoretical colours of different gravities; for $g - i > 1.0$ the gravities of the red giant branch predicted by the Besançon model (Robin et al. 2003) is followed. In our plot we explicit the gravity dependence of the index $(\text{CaHK} - g)_0 - 1.5(g - i)_0$. These theoretical colours are slightly different from those of Starkenburg et al. (2017), which were computed using a grid of MARCS models (Gustafsson et al. 2008), while these have been computed by us using the Castelli & Kurucz (2003) ATLAS9 models. The figure shows how all the stars of our sample are beyond the -4.0 theoretical curves. The Pristine metallicities are computed through a calibration process and not merely through comparison with theoretical curves, hence it is not surprising that the Pristine metallicities of all the targets are slightly below -4.0 . The model atmospheres employed to compute theoretical colours are an approximation, for instance

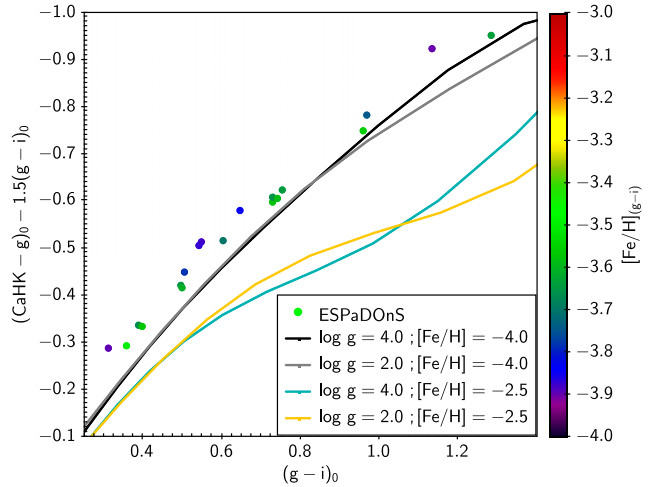


Figure 1. Colour-colour for our selected targets. The solid lines are theoretical curves for two values of metallicity and surface gravity. The points are coloured according to their photometric metallicity estimate.

both the ones that are used here and in Starkenburg et al. (2017) are one-dimensional and hydrostatic equilibrium and computed assuming Local Thermodynamic Equilibrium (LTE). It is known that granulation effects have small but not negligible effects on colours (see e.g. Bonifacio et al. 2018; Kučinskas et al. 2018), the effects of deviations from LTE are largely unexplored. Through the use of calibration stars we try to overcome the shortcomings in our theoretical colours.

3 OBSERVATIONS

The spectra were observed with ESPaDOnS (Donati et al. 2006) in the Queued Service Observation mode of CFHT between 29 November 2020 and 8 December 2020. Each star was observed twice, one exposure after the other, with exposure times that range from 1300 to 2400 s. A complete log of the observations is provide in Table 1.

The reduced data were provided to us by CFHT, the spectra are processed with the Upena.¹ pipeline using routines of the LIBRE-ESPRIT software (Donati et al. 1997). We used the ‘Star + Sky’ mode that covers the spectral range 370–1051 nm with a resolving power of 65 000. We perform the order merging using an ESO-MIDAS² script developed by us for this purpose. The script performs the order merging using the ESO-MIDAS task *merge/spec*, which computes a weighted average in the overlapping region of adjacent orders. Out of the overlaps, the spectra of adjacent orders are copied to the output spectrum. Within the overlaps, for computing the weights, our procedure uses the formula $\text{spec}_{\text{out}} = \text{spec}_1 \times (1 - c) + \text{spec}_2 \times c$, where spec_{out} is the output spectrum, spec_1 and spec_2 are the spectra of adjacent orders, and c is a ramp varying from 0 to 1 in the overlap. In this way, we recover all the information from each order. This is different from what was done in Lucchesi et al. (2022), where the overlapping regions were simply cut out and the spectra joined. In that paper, the normalized spectrum was merged. We prefer instead to use the non-normalized spectrum, since MyGIsFOS (Sbordone et al. 2014) is capable of providing an excellent pseudo-continuum and works better on non-normalized spectra, see Section 4.4 for further

¹<http://www.cfht.hawaii.edu/Instruments/Upena/>.

²<https://www.eso.org/sci/software/esomidas/>.

Table 1. Log of the observations.

star	Date (YYY MM DD)	UT (hms)	HJD (d)	T_{exp} (s)	g_0 (mag)	V_R (km s ⁻¹)	$\sigma(V_R)$ (km s ⁻¹)
Pristine_326.5701 + 19.2445	2020 11 29	04:40:55	2459182.69458	2400.0	15.323	-77.553	0.091
Pristine_326.5701 + 19.2445	2020 11 29	05:21:31	2459182.72277	2400.0		-77.434	0.088
Pristine_355.2747 + 26.4757	2020 11 29	06:09:54	2459182.75884	2400.0	13.803	-14.271	0.026
Pristine_355.2747 + 26.4757	2020 11 29	06:50:30	2459182.78705	2400.0		-14.343	0.024
Pristine_024.5944 + 25.4689	2020 11 29	09:04:03	2459182.88178	2400.0	15.247		
Pristine_024.5944 + 25.4689	2020 11 29	09:44:39	2459182.90997	2400.0			
Pristine_029.3591 + 21.3783	2020 12 03	07:14:54	2459186.80599	2400.0	14.711		
Pristine_029.3591 + 21.3783	2020 12 03	07:55:31	2459186.83420	2400.0			
Pristine_034.7189 + 25.9539	2020 12 04	10:41:09	2459187.94933	1770.3	14.116		
Pristine_034.7189 + 25.9539	2020 12 04	11:11:29	2459187.97040	1798.5			
Pristine_148.3782 + 53.0957	2020 12 04	13:11:14	2459188.05071	2222.0	14.599	23.606	0.049
Pristine_148.3782 + 53.0957	2020 12 04	13:48:55	2459188.07689	2227.7		23.503	0.050
Pristine_159.5695 + 57.1688	2020 12 04	14:47:41	2459188.11710	2393.0	14.993	-135.220	0.054
Pristine_159.5695 + 57.1688	2020 12 04	15:27:53	2459188.14502	2359.8		-135.259	0.056
Pristine_109.8329 + 41.3782	2020 12 05	11:06:51	2459188.96665	2400.0	15.149	18.360	0.015
Pristine_109.8329 + 41.3782	2020 12 05	11:47:28	2459188.99485	2400.0		18.566	0.015
Pristine_163.9735 + 13.4823	2020 12 05	14:46:24	2459189.11558	1371.3	15.195	22.88	4.17
Pristine_163.9735 + 13.4823	2020 12 05	15:09:48	2459189.13183	1363.7		30.90	6.61
Pristine_327.5170 + 19.8622	2020 12 06	04:35:28	2459189.69016	2400.0	14.930	-122.611	0.030
Pristine_327.5170 + 19.8622	2020 12 06	05:16:04	2459189.71836	2400.0		-121.771	0.030
Pristine_328.6116 + 20.3914	2020 12 06	05:58:37	2459189.74801	2400.0	15.187	-282.961	0.092
Pristine_328.6116 + 20.3914	2020 12 06	06:39:14	2459189.77621	2400.0		-284.115	0.131
Pristine_002.0937 + 22.6545	2020 12 06	07:22:25	2459189.80903	2400.0	15.268		
Pristine_002.0937 + 22.6545	2020 12 06	08:03:01	2459189.83721	2400.0			
Pristine_008.1724 + 21.8215	2020 12 06	08:45:21	2459189.86709	2400.0	15.447	-120.437	0.126
Pristine_008.1724 + 21.8215	2020 12 06	09:25:57	2459189.89529	2400.0		-120.986	0.158
Pristine_331.5576 + 27.2164	2020 12 07	04:31:50	2459190.68800	1944.8	15.041		
Pristine_331.5576 + 27.2164	2020 12 07	05:06:44	2459190.71224	2171.9			
Pristine_333.2010 + 09.6132	2020 12 07	05:48:03	2459190.74079	2400.0	15.230		
Pristine_333.2010 + 09.6132	2020 12 07	06:28:38	2459190.76898	2400.0			
Pristine_348.1325 + 11.2206	2020 12 07	07:15:53	2459190.80314	1572.5	14.444		
Pristine_348.1325 + 11.2206	2020 12 07	07:42:51	2459190.82187	1591.9			
Pristine_333.2117 + 20.1267	2020 12 08	04:27:58	2459191.68523	1544.0	14.712		
Pristine_333.2117 + 20.1267	2020 12 08	04:54:47	2459191.70385	1599.8			
Pristine_335.8411 + 09.0218	2020 12 08	05:20:47	2459191.72198	1307.7	15.471	62.307	0.059
Pristine_335.8411 + 09.0218	2020 12 08	05:43:09	2459191.73751	1304.2		63.898	0.056
Pristine_009.1439 + 15.7850	2020 12 08	06:07:40	2459191.75749	1252.4	15.483	-63.249	0.238
Pristine_009.1439 + 15.7850	2020 12 08	06:29:07	2459191.77239	1252.2		-64.053	0.193

Note. Radial velocities for SB2 stars are given in Table 2.

details. Upena corrects the spectra for the heliocentric radial velocity, so the pairs of spectra were co-added and ready for analysis.

4 ANALYSIS

4.1 Radial velocities

Before analysing the stars, we visually inspected the spectra, and this quick-look led us to suspect that some of these stars were in binary systems. We then checked for spectroscopic binaries through cross-correlation, and found that 8 out of 19 stars are SB2 binaries. To measure the radial velocities of each component, we used the technique of cross-correlation (Tonry & Davis 1979). To compute the cross-correlation functions, we use our own code that computes the cross-correlation in Fourier space using the routine `correl` (Press et al. 1992). As template we use a synthetic spectrum computed with SYNTHE from an ATLAS 9 model (Kurucz 2005). The stellar parameters are estimated as described in Section 4.3. For each star, we extracted a limited spectral range, which is detailed in

Table 2. Although the method is not applicable to binary stars, the practice showed that the derived parameters are adequate to compute a template to be used for cross-correlation. Finally, the velocity of each component is estimated by fitting two gaussians to the cross-correlation peaks, using the IRAF³ task `splot` with the deblending option. The radial velocities can be found in Table 2, the uncertainties are estimated as described in Tonry & Davis (1979). For each star, we call ‘A’ component the one with the highest peak in the cross-correlation function. For stars that did not show sign of a secondary spectrum, we measured the radial velocity with our own template matching code, and the velocities can be found in Table 1. Template matching is a technique in which a template spectrum is matched to an observed spectrum by minimizing a χ^2 function in which the radial velocity is one of the fitting parameters, it is described for example in Koposov et al. (2011). We use our own code to perform template matching, in which the radial velocity is the only free parameter. We normalize the observed spectrum by

³<https://iraf-community.github.io>.

Table 2. Radial velocities for SB2 binaries.

ID	HJD (d)	$V_R(A)$ (km s ⁻¹)	$\sigma[V_R(A)]$ (km s ⁻¹)	$V_R(B)$ (km s ⁻¹)	$\sigma[V_R(B)]$ (km s ⁻¹)	CCF template $T_{\text{eff}}/\log g/\text{metallicity}$	CCF range (nm)
Pristine_002.0937 + 22.6545	2459189.80903	-61.27	0.83	11.31	0.87	5400/4.0/-1.0	500–580
Pristine_002.0937 + 22.6545	2459189.83721	-54.68	2.33				500–580
Pristine_024.5944 + 25.4689	2459182.88178	-138.30	6.00	166.60	5.60	5000/4.0/-1.0	470–582
Pristine_024.5944 + 25.4689	2459182.90997	-138.30	5.60	145.10	5.40		470–582
Pristine_029.3591 + 21.3783	2459186.80599	71.70	6.80	-212.70	3.20	5600/4.0/-1.0	470–582
Pristine_029.3591 + 21.3783	2459186.83420	83.80	6.80	-243.70	3.60		470–582
Pristine_034.7189 + 25.9539	2459187.94933	-12.00	2.90	269.10	1.60	5800/4.0/-1.0	410–565
Pristine_034.7189 + 25.9539	2459187.97040	-20.50	4.40	282.30	2.30		410–565
Pristine_331.5576 + 27.2164	2459190.68800	66.09	5.90	-253.58	3.60	5600/4.0/-1.0	470–582
Pristine_331.5576 + 27.2164	2459190.71224	65.88	6.60	-194.60	4.60	470–582	
Pristine_333.2010 + 09.6132	2459190.74079	-25.63	0.28	71.83	0.40	5400/4.0/-1.0	470–582
Pristine_333.2010 + 09.6132	2459190.76898	-31.07	0.33	77.05	0.94		470–582
Pristine_333.2117 + 20.1267	2459191.68523	43.50	6.01	-256.85	3.30	5800/4.0/-1.0	470–582
Pristine_333.2117 + 20.1267	2459191.70385	67.58	7.10	-262.50	3.50		470–582
Pristine_348.1325 + 11.2206	2459190.80314	-13.68	0.25	12.43	0.23	5800/4.0/-1.0	475–579
Pristine_348.1325 + 11.2206	2459190.82187	-15.08	0.23	13.41	0.23		475–579
Pristine_181.3698 + 117645 ^a	2457447.10106	78.87	0.17	-42.19	0.18	5400/3.00/-1.5	471–580
Pristine_213.2814 + 14.8983 ^b	2457819.15463	-8.94	0.29	-20.16	0.43	6000/3.50/-2.0	600–655
Pristine_254.3844 + 12.9652 ^c	2457887.02381	-379.71	0.26	-391.79	0.21	5200/3.00/-2.5	600–655
Pristine_254.3844 + 12.9652 ^c	2457887.05204	-378.10	0.23	-390.84	0.22		600–655

Note. Stars marked with \star are the three stars (four spectra) in the Lucchesi et al. (2022) sample, classified as fast rotators by the authors. ^aThis star is named Pristine_181.3708 + 11.7636 in Lucchesi et al. (2022) and is also present in Venn et al. (2020) with the SDSS coordinates RA = 181.3699, Dec. = +11.7636.

^bThis star is also present in Venn et al. (2020); in this case, Pristine and SDSS are identical, to four decimal places.

^cIn Lucchesi et al. (2022), this star is named Pristine_254.3844 + 12.9653

fitting a spline through interactively chosen continuum points using an updated version of the *NORMA* code (Bonifacio 1989). As template, we use a synthetic spectrum computed with the parameters derived as described in Section 4.3. Koposov et al. (2011) argued that template matching performs better than cross-correlation, provided that the template is close to the observed spectrum, and this is confirmed by our own tests. One basic limitation of cross-correlation was pointed out by Tonry & Davis (1979): the error estimate they provide, and that we use, does not take into account the template mismatch. The contribution to the error of template mismatch increases as the signal-to-noise ratio (S/N) increases and eventually dominates the total error. For this reason cross-correlation is often the method of choice for single spectrum spectroscopy binaries (SB1) and planet hunting, in which case, from a series of low S/N spectra one can produce, by co-addition, a high S/N spectrum, to be used as template (see e.g. Aguado et al. 2022, 2023). The advantage of template matching is that the total error is estimated taking into account the mismatch between the template and the spectrum. One disadvantage of template matching is that if the mismatch is large, for example a temperature difference of the order of 500 K, the minimization procedure can get trapped in a secondary minimum, which is very far from the true radial velocity. For further discussion on the comparison between cross-correlation and template-matching we refer the reader to Rix & White (1992) and Cappellari & Emsellem (2004).

We do not provide parameters nor perform chemical analysis for any of the SB2 binaries (Table 2), since to disentangle the spectra we need information on the luminosities of the two star (see e.g. Venn et al. 2003; González Hernández et al. 2008). This information may come from the orbital solution, combined with theoretical isochrones. We thus defer such an analysis to when an orbital solution, and therefore a mass function, of the system shall be available. We also do not chemically analyse the stars Pristine_109.8329 + 41.3782, Pristine_148.3782 + 53.0957, Pristine_163.9735 + 13.4823, and

Pristine_326.5701 + 19.2445, because they are rotating rapidly and the S/N is too low ($S/N \sim 5$ at 550 nm) to allow for a proper analysis (see Section 5.2 for more details). Further details on the 12 non-analysed stars are provided in Section 5.2, and in the last but one column of Table 3, the stars are marked as ‘N’. The uncertainties in radial velocity are the formal uncertainties derived from the χ^2 in case of the template matching and from the Tonry & Davis (1979) formalism for cross-correlation. To these uncertainties, which are of statistical nature, one should add a systematic of 0.02 km s⁻¹, for the stability of ESPaDOnS⁴. In several cases the difference in radial velocity between the two consecutive exposures is larger than the combined statistical and systematic uncertainties. We believe that these variations are real, as is surely the case for the two RR Lyrae stars observed, which show clear radial velocity variations.

Lucchesi et al. (2022) homogeneously analysed a sample of Pristine metal-poor candidates observed with ESPaDOnS. The majority of the Lucchesi et al. (2022) observations are described in Venn et al. (2020), which also provides an independent homogeneous analysis. Three stars in Lucchesi et al. (2022) sample were excluded from the analysis and labelled as ‘fast rotators’, two of which had already been analysed by Venn et al. (2020). Since the targets in Venn et al. (2020) and Lucchesi et al. (2022) were selected in a similar way to ours, we looked at the spectra of these three stars to see if they could be variables or SB2 binaries. In deriving the radial velocities by cross-correlation, we found that these stars show a double peak in the cross-correlation function, thus suggesting that they are SB2 binaries. The last four rows of Table 2 provide the radial velocities we measured for these three stars in Lucchesi et al. (2022) from the two peaks of the cross-correlation function. For star Pristine_181.3708 + 11.7636, the two peaks are well distinct, while for the other stars

⁴http://www.ast.obs-mip.fr/projets/espadons/espadons_new/stability.html.

Table 3. Stars observed with ESPaDoNS in period 20B.

Star	RA(CaHK) ($^{\circ}$)	Dec.(CaHK) ($^{\circ}$)	DR3 name	G (mag)	$G_{BP} - G_{RP}$ (mag)	A/N	Comment
Pristine.002.0937 + 22.6545	2.093 724 97	+ 22.654 527 66	<i>Gaia</i> DR3 2 847 119 325 004 632 960	14.590	1.024	N	SB2, ECL ^{1,2,3}
Pristine.008.1724 + 21.8215	8.172 4329	+ 21.821 502 69	<i>Gaia</i> DR3 2 799 728 346 622 900 480	15.252	0.700	A	
Pristine.009.1439 + 15.7850	9.143 9209	+ 15.785 063 74	<i>Gaia</i> DR3 2 780 656 630 244 179 712	15.371	0.692	A	
Pristine.024.5944 + 25.4689	24.594 478 61	+ 25.468 952 18	<i>Gaia</i> DR3 292 459 170 887 172 352	14.471	1.253	N	SB2, ECL ^{1,2,3,4,5,6,7}
Pristine.029.3591 + 21.3783	29.359 157 56	+ 21.378 3741	<i>Gaia</i> DR3 97 471 675 738 184 576	14.474	0.910	N	SB2, ECL ^{3,7,8}
Pristine.034.7189 + 25.9539	34.718 940 73	+ 25.953 910 83	<i>Gaia</i> DR3 106 031 957 876 177 024	13.881	0.848	N	SB2, ECL ^{3,7,9}
Pristine.109.8329 + 41.3782	109.832 969 67	+ 41.378 276 82	<i>Gaia</i> DR3 948 549 265 398 560 512	14.844	0.940	N	ECL ^{2,6}
Pristine.148.3782 + 53.0957	148.378 204 35	+ 53.095 771 79	<i>Gaia</i> DR3 828 505 655 325 207 680	13.562	1.207	N	RS CVn ³
Pristine.159.5695 + 57.1688	159.569 595 34	+ 57.168 876 65	<i>Gaia</i> DR3 853 989 036 322 676 224	14.334	1.129	A	
Pristine.163.9735 + 13.4823	163.973 526	+ 13.482 327 46	<i>Gaia</i> DR3 3 872 789 126 248 434 560	14.668	0.772	N	ECL ^{3,8}
Pristine.326.5701 + 19.2445	326.570 190 43	+ 19.244 558 33	<i>Gaia</i> DR3 1 780 400 940 765 306 624	14.509	1.500	N	RS CVn ^{3,4}
Pristine.327.5170 + 19.8622	327.517 059 33	+ 19.862 203 6	<i>Gaia</i> DR3 1 780 495 017 728 775 680	15.014	0.913	A	RS CVn ^{1,10} , ECL ^{2,3}
Pristine.328.6116 + 20.3914	328.611 694 34	+ 20.391 477 58	<i>Gaia</i> DR3 1 780 903 486 298 463 872	14.953	1.009	A	
Pristine.331.5576 + 27.2164	331.557 678 22	+ 27.216 463 09	<i>Gaia</i> DR3 1 892 821 297 421 984 128	14.628	0.988	N	SB2, ECL ^{2,3}
Pristine.333.2010 + 09.6132	333.201 0498	+ 9.613 277 44	<i>Gaia</i> DR3 2 723 881 217 040 192 640	14.545	1.041	N	SB2, ECL ²
Pristine.333.2117 + 20.1267	333.211 761 47	+ 20.126 791	<i>Gaia</i> DR3 1 778 301 217 153 109 760	14.294	0.849	N	SB2, ECL ^{1,3,4} , RR-Lyr ¹¹
Pristine.335.8411 + 09.0218	335.841 186 52	+ 9.021 878 24	<i>Gaia</i> DR3 2 723 074 347 304 080 384	15.223	0.727	A	RR-Lyr ^{3,6,9,10,11}
Pristine.348.1325 + 11.2206	348.132 507 32	+ 11.220 616 34	<i>Gaia</i> DR3 2 810 661 890 249 732 480	13.813	0.816	N	SB2, ECL ¹²
Pristine.355.2747 + 26.4757	355.274 749 76	+ 26.475 736 62	<i>Gaia</i> DR3 2 864 940 415 627 238 784	13.645	0.942	A	

Notes. Label A indicates the stars that have been chemically analysed, while label N indicates the stars that have not. The abbreviation ECL stands for eclipsing binary, SB2 stands for double-lined spectroscopic binary, RS CVn stands for RS Canum Venaticorum stars, and RR Lyr stands for RR Lyrae. *References.* ¹ Watson, Henden & Price (2006), ² Jayasinghe et al. (2018), ³ Gaia Collaboration et al. (2022), ⁴ Chen et al. (2018), ⁵ Tian et al. (2020), ⁶ Heinze et al. (2018), ⁷ Marsh et al. (2017), ⁸ Sun et al. (2020), ⁹ Drake et al. (2014), ¹⁰ Chen et al. (2020), ¹¹ Sesar et al. (2017), ¹² Ferreira Lopes et al. (2015).

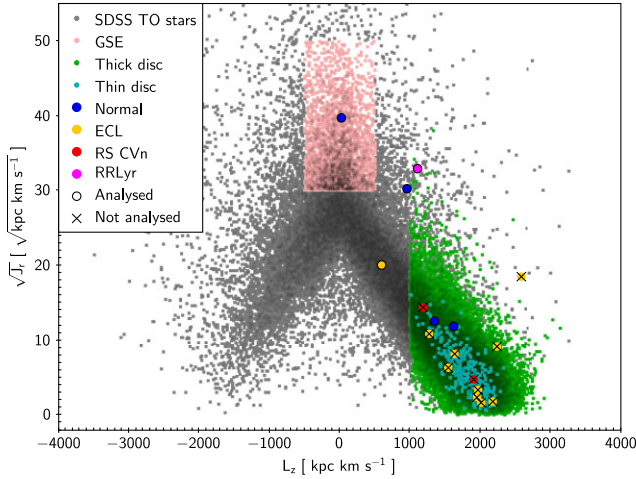


Figure 2. The L_z – $\sqrt{J_r}$ plane for our sample of stars. The properties of our stars are specified in the legend. The grey dots that we use as reference stars are the Turn Off stars from Bonifacio et al. (2021). Further details can be found in the text.

the two peaks are only visible in the red part of the spectra, in the 600–655 nm range. In our opinion, the absence of the second peak in the blue part of the spectra could mean that the companion is cooler and, therefore, less observable in the blue. However, the absence of the second peak in the blue could be also due to the fact that the S/N ratio is too low and the lines of the secondary are not detectable. Star Pristine_213.2814 + 14.8983 has also been identified as an RR Lyrae with a period of 0.63 d by several studies (Drake et al. 2013; Sesar et al. 2013, 2017; Abbas et al. 2014; Greer et al. 2017; Heinze et al. 2018).

4.2 Kinematics

With our radial velocities and the *Gaia* DR3 (Gaia Collaboration et al. 2022) parallaxes and proper motions we compute the actions for our sample of stars, as done in Kordopatis et al. (2023). The actions were computed with the code *Galpy* (Bovy 2015), in combination with the axisymmetric potential of McMillan (2017) adapted to the solar position (R, Z)_⊙ = (8.249, 0.0208) kpc and velocities (V_r, V_ϕ, V_z)_⊙ = (−9.5, 250.7, 8.56) km s^{−1}. The parallaxes were corrected for the zero point according to the prescriptions of Lindegren et al. (2021). For the SB2 stars, we took as radial velocity the mean of the velocities of the two peaks in the cross-correlation function, which is the velocity of the centre of mass of the system. For the stars that are recognized as binaries by *Gaia*, proper motions and parallaxes take into account the orbital motion (Halbwachs et al. 2022). For the RR Lyrae star, we use the mean observed radial velocity since we do not have a radial velocity curve available.

In Fig. 2, we plot the angular momentum (L_z) versus radial action ($\sqrt{J_r}$) for our sample of stars and use as background reference the sample of Bonifacio et al. (2021). Stars that fall in the Gaia-Sausage-Enceladus accretion event (Belokurov et al. 2018; Haywood et al. 2018; Helmi et al. 2018, GSE hereafter) according to the kinematic selection criterion of Feuillet et al. (2020).⁵ are coloured in pink. It should be noted that the solar position and velocity adopted by Feuillet et al. (2020) and Kordopatis et al. (2023) are slightly different, the most significant difference being the velocity in the

direction of the Galactic rotation that is assumed to be 220 km s^{−1} by Feuillet et al. (2020) and 250.7 km s^{−1} by Kordopatis et al. (2023). We did not attempt to change the range in L_z defining the GSE to reflect this fact, since it is not important for our discussion. Thick disc stars are coloured in green⁶ Thin disc stars.⁷ are coloured in light blue. Stars in our sample that have not been analysed are covered by a black × sign, eclipsing binaries (ECL) are shown as yellow dots, RS Canum Venaticorum stars (RS CVns) as red dots, and the RR Lyrae (RR Lyr) is shown as magenta circle. Most of the eclipsing binaries and both of the RS CVns are found in the thin disc. Only one eclipsing binary is found in the thick disc.

The two most metal-poor stars and the RR Lyrae star are unsurprisingly found to have low L_z and high J_r , what a few years ago one would have described as ‘halo’ orbits. However it is remarkable that one of the two most metal-poor stars found in our sample, Pristine_159.5695 + 57.1688 ([Fe/H] ∼ −3.1), is clearly in the region occupied by the GSE structure. One should however keep in mind the error on the parallax of this star is large ($\Delta\varpi \approx 59$ per cent). This is the largest uncertainty on the Galactic orbit of this star; therefore, it is also uncertain whether it belongs to GSE or not. There is a debate on the metallicity distribution function (MDF) of the GSE, with Feuillet et al. (2020) and Naidu et al. (2020) favouring an MDF peaking at metallicity −1.0 and a quick drop providing essentially no stars below −3.0, while Bonifacio et al. (2021) show an MDF peaking at −1.8. There are other indications in the literature for a low metallicity component in GSE. Based on a smaller samples, with respect to the above cited investigations, Matsuno, Aoki & Suda (2019) and Myeong et al. (2019) found that the MDF of GSE peaks around −1.3. Monty et al. (2020) associate to GSE a star with [Fe/H] ≤ −3.5 as can be appreciated by their Fig. 11. Since our sample is clearly biased in favour of low metallicity stars we should compare with the MDF of (Bonifacio et al. 2021) not corrected for the bias. That MDF has in fact a sizeable fraction of stars below −3, while no stars this metal-poor should be observed if the MDF were as proposed by Feuillet et al. (2020) or Naidu et al. (2020). Two things should be borne in mind: (i) A purely kinematical selection of GSE, like shown in Fig. 2, will have about 20 per cent contamination (Bonifacio et al. 2021), thus the fact that Pristine_159.5695 + 57.1688 is in that region of action space does not guarantee that it is a member of GSE; (ii) it is possible that the differences among the GSE MDFs found in the literature are rooted in the different selection functions of the samples used to derive the MDFs. The issue of separating stellar populations by chemical or dynamical means has become the object of many investigations (see e.g. Franchini et al. 2020; Buder et al. 2022; Lane, Bovy & Mackereth 2022). Especially relevant here is figure 9 of Buder et al. (2022), where they show how a purely chemical or purely dynamical selection of GSE differ and overlap.

4.3 Stellar parameters

To derive the stellar parameters for our sample of stars, we use the *Gaia* Data Release 3 (DR3) photometry ($G, G_{BP} - G_{RP}$) and parallaxes (Gaia Collaboration et al. 2016, 2022) adopting the same procedure described in Lombardo et al. (2021). The grid of ATLAS 9 model atmosphere we use to derive stellar parameters has effective temperatures (T_{eff}), and surface gravities ($\log g$) in the range $3500 \leq T_{\text{eff}} \leq 6750$ K, $0.5 \leq \log g \leq 5.0$ dex, with a step of 250 K in T_{eff} , and 0.5 dex in $\log g$, for metallicities [M/H] = −4, −2.5, −2.0,

⁵ $-500 < L_z < 500$ kpc km s^{−1} and $30 < \sqrt{J_r} < 50$ (kpc km s^{−1})^{1/2}.

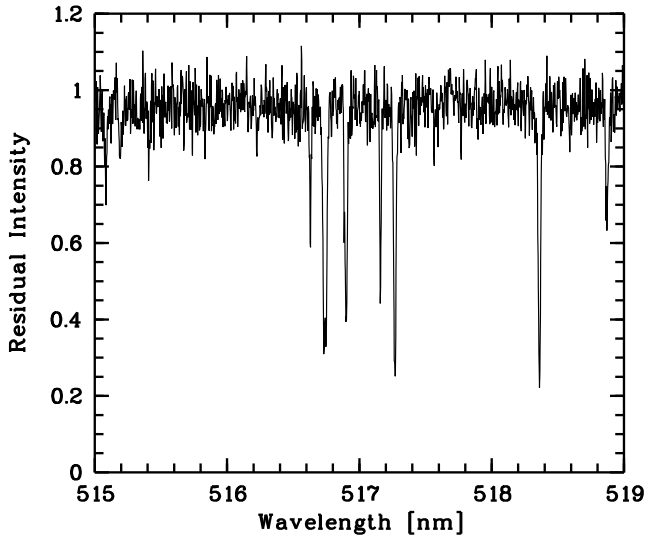
⁶ $L_z < 1000$ kpc km s^{−1} and $z_{\text{max}} < 3.0$ kpc.

⁷ $L_z < 1000$ kpc km s^{−1} and $z_{\text{max}} < 0.3$ kpc.

Table 4. Derived stellar parameters for stars analysed chemically.

ID	T_{eff} (K)	$\log g$ (dex)	v_t (km s $^{-1}$)	[Fe I/H] (dex)	[Fe II/H] (dex)	[Fe/H] $_{gi}$ (dex)	[Fe/H] $_{gr}$ (dex)	S/N @ 550 nm
Pristine_008.1724 + 21.8215	6051	2.39	2.07	-1.87 ± 0.16 (20)	-1.91 ± 0.08 (2)	-3.52	-3.56	12
Pristine_009.1439 + 15.7850	6278	4.29	1.29		-2.58 ± 0.20 (1)	-3.90	-3.81	10
Pristine_159.5695 + 57.1688	4798	1.42	2.06	-3.07 ± 0.19 (43)	-3.23 ± 0.14 (5)	-3.74	-3.52	28
Pristine_327.5170 + 19.8622	5817	2.53	1.91	-1.76 ± 0.20 (46)	-1.57 ± 0.20 (3)	-3.67	-3.51	18
Pristine_328.6116 + 20.3914	5245	2.87	1.62	-3.56 ± 0.17 (5)		-3.85	-3.63	13
Pristine_335.8411 + 09.0218	6091	2.88	1.88	-1.68 ± 0.17 (28)	-1.12 ± 0.17 (5)	-3.58	-3.55	12
Pristine_355.2747 + 26.4757	5586	4.10	0.98	-0.66 ± 0.13 (147)	-0.47 ± 0.16 (19)	-3.88	-3.72	30

Notes. [Fe I/H] and [Fe II/H] are the iron abundances derived with MyGIsFOS. [Fe/H] $_{gi}$ and [Fe/H] $_{gr}$ are the metallicities estimated with the Pristine photometry combined with the $(g - i)$ and $(g - r)$ colours, respectively. In columns 5 and 6, the number of lines is reported in parentheses.

**Figure 3.** The region of Mg I b triplet in star Pristine_159.5695 + 57.1688.

$-1.5, -1.0, -0.5, +0.0, +0.2, +0.5$. The α -elements are enhanced by $+0.4$ for models with $[M/H] \leq -1$ and solar-scaled for the others. The micro-turbulent velocity is 2 km s^{-1} for all models. The *Gaia* parallaxes are corrected for the zero point according to Lindegren et al. (2021). We adopted the reddening values provided by Schlafly & Finkbeiner (2011) maps. Micro-turbulent velocities are derived using the empirical calibration in Mashonkina et al. (2017). The derived stellar parameters for our sample stars are listed in Table 4.

4.4 Chemical abundances

We were able to derive the chemical abundances for 7 out of 19 stars in our sample. A portion of one of our higher S/N ratio spectra (S/N = 28 at 550 nm), that of Pristine_159.5695 + 57.1688, is shown in Fig. 3. This star is also one of the two most metal-poor in the sample. The abundances are derived using MyGIsFOS (Sbordone et al. 2014). Our adopted solar abundances are from Caffau et al. (2011) and from Lodders, Palme & Gail (2009) for all the elements not included in Caffau et al. (2011). MyGIsFOS performs a line-by-line χ^2 fitting on selected spectral features, interpolating in a pre-computed grid of synthetic spectra. We use synthetic grids computed from a grid of ATLAS 12 model atmospheres, using the SYNTHE code (Kurucz 2005). This method has already been used and described in several of the Pristine papers (Caffau et al. 2017; Starkenburg et al. 2018; Bonifacio et al. 2019; Caffau et al. 2020). The atomic data for

the spectrum synthesis are taken from Heiter et al. (2021). The molecular data are taken from the site of R.L. Kurucz⁸, including the CH lines by Masseron et al. (2014)⁹. We stress that, by fitting synthetic spectra, MyGIsFOS takes into account all the blending features, in this respect it is different from codes that use equivalent widths to derive abundances. The analysed stars are present in several catalogues, but no chemical analysis is available in the literature. In this study, the chemical abundances of these star are provided for the first time. The derived abundances are listed in Table 5.

In Figs 4, 5, 6, and 7, we show [Mg/Fe], [Ca/Fe], [Sc/Fe], and [Ba/Fe] abundance ratios as a function of [Fe/H]. As reference, we have taken the stars of the ESO Large Programme ‘First Stars’ (Cayrel et al. 2004; François et al. 2007), of Ishigaki et al. (2012); Ishigaki et al. (2013), of papers Pristine V (Bonifacio et al. 2019) and Pristine XV (Lucchesi et al. 2022), and of Lombardo et al. (2022).

Ca has been measured in five out of seven stars. In our sample, star Pristine_327.5170 + 19.8622 has [Ca/Fe] = $+0.6$, which is slightly higher than the reference samples values (Fig. 5). However, this star has [Mg/Fe] = $+0.3$ (Fig. 4), and, taking into account the uncertainties, this appears to be consistent with an average $[\alpha/\text{Fe}] \sim +0.4$.

We could measure the Sc abundance for five out of seven stars. One remarkable star is the most metal-rich star of the sample, Pristine_355.2747 + 26.4757, which has [Sc II/Fe II] = $+0.49$. Since the measure is based on seven Sc II lines with a line-to-line scatter of 0.1 dex, we consider the measure precise. Although the Sc abundance in Pristine_355.2747 + 26.4757 is higher than that in the other stars in the sample, it is still compatible with the values found in the literature for stars of similar metallicity, as shown in Fig. 6. Another remarkable star is Pristine_335.8411 + 09.0218, which shows [Sc II/Fe II] = -0.15 . However, we note that, for this star, the Sc abundance is $A(\text{Sc II}) = 1.83$, while [Fe II/H] = -1.12 , which is 0.55 dex higher than [Fe I/H]. This value is similar to the Sc abundance derived for Pristine_327.5170 + 19.8622, $A(\text{Sc II}) = 1.70$, which has [Fe/H] = -1.76 .

We are able to measure Ba for six out of seven stars, for four of which two Ba II lines could be measured. As shown in Fig. 7, when compared with other stars in the literature, five out of six of our [Ba/Fe] measurements seem compatible with those of other stars at similar metallicity. The possibly odd star is Pristine_327.5170 + 19.8622, which appears to display a higher [Ba/Fe] than stars of similar metallicity. It would be interesting to

⁸<http://kurucz.harvard.edu/linelists/linesmol/>.

⁹<http://kurucz.harvard.edu/molecules/ch/>.

Table 5. Derived chemical abundances for analysed stars.

Star	A(Na) $\pm\sigma$ (N)	A(Mg) $\pm\sigma$ (Mg) (N)	A(Al) $\pm\sigma$ (Al) (N)	A(Si I) $\pm\sigma$ (Si I) (N)	A(Si II) $\pm\sigma$ (Si II) (N)	A(Ca) $\pm\sigma$ (Ca) (N)
Pristine_008.1724 + 21.8215						4.91 \pm 0.08 (5)
Pristine_009.1439 + 15.7850						
Pristine_159.5695 + 57.1688	3.22 \pm 0.20 (1)	5.07 \pm 0.17 (2)				3.70 \pm 0.11 (5)
Pristine_327.5170 + 19.8622		6.10 \pm 0.20 (1)				5.16 \pm 0.21 (9)
Pristine_328.6116 + 20.3914		4.71 \pm 0.20 (1)				
Pristine_335.8411 + 09.0218		6.15 \pm 0.20 (1)				4.89 \pm 0.17 (5)
Pristine_355.2747 + 26.4757	5.79 \pm 0.03 (3)	7.33 \pm 0.20 (1)	6.03 \pm 0.20 (1)	7.14 \pm 0.03 (8)	7.52 \pm 0.20 (1)	5.92 \pm 0.07 (8)
	A(Sc II) $\pm\sigma$ (Sc II) (N)	A(Ti I) $\pm\sigma$ (Ti I) (N)	A(Ti II) $\pm\sigma$ (Ti II) (N)	A(V) $\pm\sigma$ (V) (N)	A(Cr I) $\pm\sigma$ (Cr I) (N)	A(Cr II) $\pm\sigma$ (Cr II) (N)
Pristine_008.1724 + 21.8215	1.34 \pm 0.20 (1)		3.40 \pm 0.20 (1)			
Pristine_009.1439 + 15.7850						
Pristine_159.5695 + 57.1688	0.14 \pm 0.18 (3)	1.94 \pm 0.19 (2)	2.11 \pm 0.07 (5)			
Pristine_327.5170 + 19.8622	1.70 \pm 0.17 (5)		3.73 \pm 0.18 (5)		3.69 \pm 0.20 (1)	
Pristine_328.6116 + 20.3914						
Pristine_335.8411 + 09.0218	1.83 \pm 0.20 (1)	3.84 \pm 0.20 (1)	3.71 \pm 0.23 (2)			
Pristine_355.2747 + 26.4757	3.13 \pm 0.10 (7)	4.51 \pm 0.07 (16)	4.79 \pm 0.17 (17)	3.36 \pm 0.07 (4)	4.95 \pm 0.11 (8)	5.37 \pm 0.20 (5)
	A(Mn) $\pm\sigma$ (Mn) (N)	A(Co) $\pm\sigma$ (Co) (N)	A(Cu) $\pm\sigma$ (Cu) (N)	A(Zn) $\pm\sigma$ (Zn) (N)	A(Y II) $\pm\sigma$ (Y II) (N)	A(Ba II) $\pm\sigma$ (Ba II) (N)
Pristine_008.1724 + 21.8215						0.36 \pm 0.07 (2)
Pristine_009.1439 + 15.7850						
Pristine_159.5695 + 57.1688						
Pristine_327.5170 + 19.8622					0.65 \pm 0.02 (2)	
Pristine_328.6116 + 20.3914						
Pristine_335.8411 + 09.0218						
Pristine_355.2747 + 26.4757	4.59 \pm 0.15 (10)	4.45 \pm 0.25 (2)	3.51 \pm 0.11 (2)	4.30 \pm 0.15 (2)	1.35 \pm 0.20 (1)	0.85 \pm 0.08 (2)
						1.64 \pm 0.31 (2)

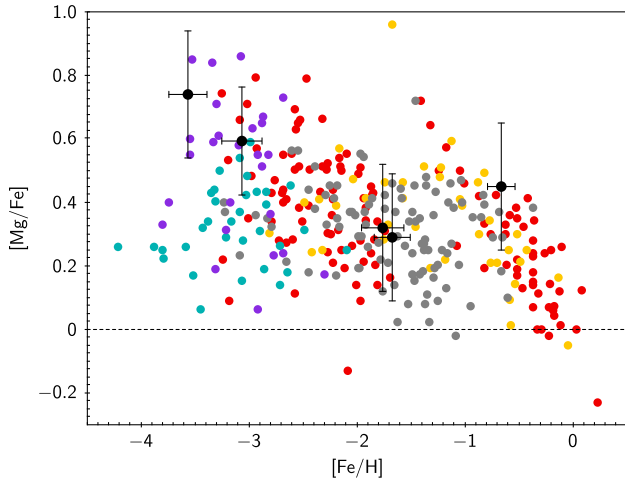


Figure 4. $[\text{Mg}/\text{Fe}]$ as a function of $[\text{Fe}/\text{H}]$ for our sample stars (black dots). Red dots are the stars from the Pristine XV paper (Lucchesi et al. 2022), yellow dots are from the Pristine V paper (Bonifacio et al. 2019), magenta dots are from the Pristine II paper (Caffau et al. 2017), purple dots are from the Pristine XII paper (Kielty et al. 2021), cyan dots are from Cayrel et al. (2004), and grey dots are from Ishigaki, Chiba & Aoki (2012).

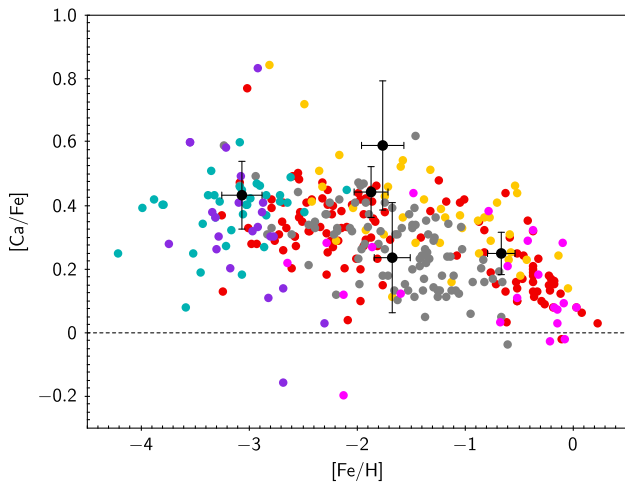


Figure 5. $[\text{Ca}/\text{Fe}]$ as a function of $[\text{Fe}/\text{H}]$ for our sample stars (black dots). The other symbols are like in Fig. 4.

measure abundances of other n -capture elements in this star. As discussed below, this star is a binary of RS CVn type.

5 REMARKS ON INDIVIDUAL STARS

5.1 Stars with chemical analysis

We first discuss the information in the literature we found for stars for which we performed a chemical analysis.

5.1.1 Pristine_009.1439 + 15.7850

The star was classified from its spectrum as a subdwarf A star (sdA)¹⁰ with $T_{\text{eff}} = 6926$ K and $\log g = 5.48$ dex by Kepler et al. (2016).

¹⁰According to Kepler et al. (2016), sdA stars show hydrogen-dominated spectra with $5.5 \leq \log g \leq 6.5$ dex and $T_{\text{eff}} \leq 20\,000$ K.

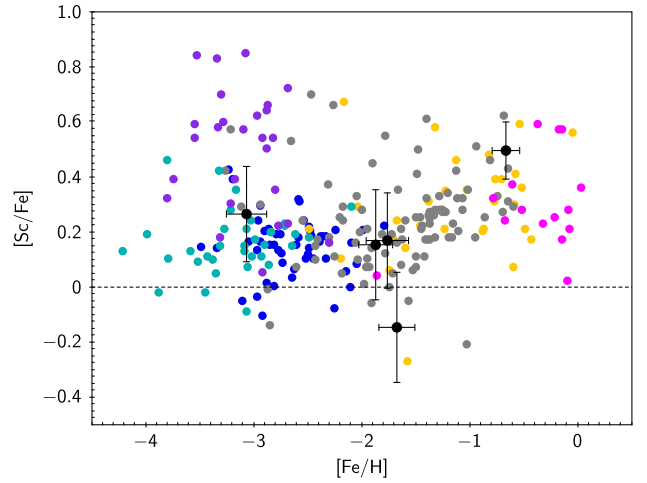


Figure 6. $[\text{Sc}/\text{Fe}]$ as a function of $[\text{Fe}/\text{H}]$ for our sample stars (black dots). Blue dots are the stars from Lombardo et al. (2022), yellow dots are from the Pristine V paper (Bonifacio et al. 2019), magenta dots are from the Pristine II paper (Caffau et al. 2017), purple dots are from the Pristine XII paper (Kielty et al. 2021), cyan dots are from Cayrel et al. (2004), and grey dots are from Ishigaki, Aoki & Chiba (2013).

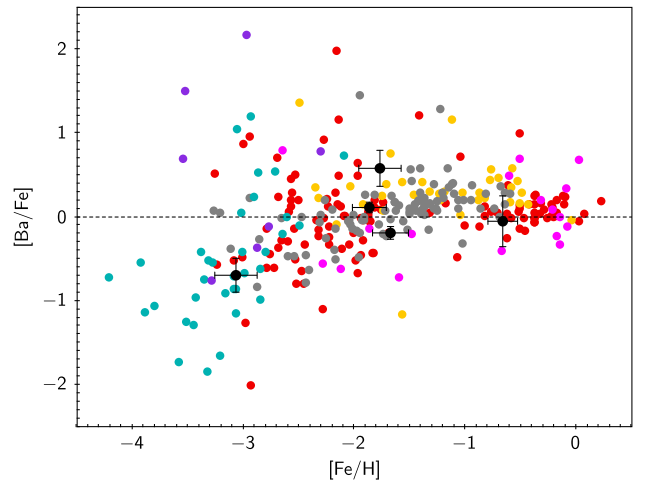


Figure 7. $[\text{Ba}/\text{Fe}]$ as a function of $[\text{Fe}/\text{H}]$. Red dots are the stars from the Pristine XV paper (Lucchesi et al. 2022), yellow dots are from the Pristine V paper (Bonifacio et al. 2019), magenta dots are from the Pristine II paper (Caffau et al. 2017), purple dots are from the Pristine XII paper (Kielty et al. 2021), cyan dots are from François et al. (2007), and grey dots are from Ishigaki et al. (2013).

This effective temperature and gravity are inconsistent with *Gaia* photometry and parallaxes, and from our high-resolution spectrum. We classify it as metal-poor G dwarf.

5.1.2 Pristine_327.5170 + 19.8622

Watson et al. (2006) classify this star as an RS CVn variable, and provide a period of 0.914 7628 d and an amplitude of 0.116 mag. Also, Chen et al. (2020) classify it as an RS CVn variable, with the same period and a 0.128 mag amplitude. This star was identified as a variable with a period of 1.829 439 d by Heinze et al. (2018). According to Jayasinghe et al. (2018), this star is an eclipsing W

Ursae Majoris-type binary¹¹, with an amplitude of 0.18 mag and a period of 1.829 4812 d. The star is also present in the *Gaia* DR3 catalogue as an eclipsing binary, with a period of 1.829 375 d and an amplitude of variation in the *G* band of 0.122 mag. The period provided by Heinze et al. (2018), Jayasinghe et al. (2018), and *Gaia* DR3 is probably an alias of the shorter period provided by other catalogues. Our two 40-min exposures display a difference in radial velocity that is of almost 1 km s^{-1} supporting the notion of a rather short period. Assuming the shorter period one can guess a velocity amplitude of 16 km s^{-1} . RS CVn binaries are systems in which the primary is a giant or sub-giant of type F to K and the secondary is a dwarf of type G to M (see e.g. Martínez, Mauas & Buccino 2022, and references therein). The spectral parameters we derived for this star are consistent with a giant of G-type; however, its low metallicity makes it more likely a Horizontal Branch star. RS CVn stars are generally very active chromospherically and strong X-ray emitters. Our spectrum is of too low S/N ratio around Ca II H&K lines to detect any core emission (S/N < 2), and we do not find emission in H α or other signs of chromospheric activity. We searched the Second ROSAT all-sky survey (2RXS) source catalogue (Boller et al. 2016), but we could not find any X-ray source within 2 arcmin from this star. We believe that this star is not an RS CVn star, at least in the classical sense. Other known RS CVn are at most moderately metal-poor (see e.g. Randich, Giampapa & Pallavicini 1994) and this star, to our knowledge, would be the most metal-poor known RS CVn.

5.1.3 *Pristine_335.8411 + 09.0218*

Several studies have identified this star as a fundamental-mode RR Lyrae variable (RRab) (Drake et al. 2014; Sesar et al. 2017; Heinze et al. 2018; Chen et al. 2020) with a period of ~ 0.67 d. Drake et al. (2014) find a period of 0.672 505 d with a *V* magnitude amplitude of 0.23 mag. The star is listed in the *Gaia* DR2 RR Lyrae catalogue as an RRab with a period of 0.672 518 54 d and a peak-to-peak *G* magnitude variability of 0.241 601 mag. In the *Gaia* DR3 RR Lyrae catalogue, the star is listed as an RRab with a period of 0.672 527 d and a peak-to-peak *G* magnitude variability of 0.244 541 59 mag. Our two spectra taken at about a 22-min distance show a variation in the radial velocity of about 1.5 km s^{-1} . We checked the light curve of the star and interpolated the colour using the observation date, which implies a phase of 0.18. The effective temperature thus derived was just 40 K hotter than that derived using the mean *Gaia* colour. We also tried to determine the effective temperature from the excitation equilibrium, but we have too few iron lines and the iteration does not converge. Our spectroscopic metallicity is in stark disagreement with that provided by *Gaia* DR3 from the Fourier decomposition of the *G* light curve (see Clementini et al. 2022, and references therein). *Gaia* DR3 provides $[M/H] = -0.15 \pm 0.34$ to be compared with our $[Fe/H] = -1.68 \pm 0.17$. Although our iron abundance is based on only 28 lines, we consider it robust and uncertainties in the adopted effective temperature, as discussed above, cannot bridge the about 1 dex difference with the *Gaia* DR3 metallicity. Also, star *Pristine_213.2814 + 14.8983* in the Venn et al. (2020) and Lucchesi et al. (2022) sample is an RR Lyr. It is in the *Gaia* DR3 catalogue, with an estimated metallicity from the Fourier decomposition of

¹¹According to the General Catalogue of Variable Stars Samus' et al. (2017), this type of eclipsing binaries, of which W UMa is the prototype, are short period (< 1 d), in contact, so that the components have an ellipsoidal shape. The light curve is such that it is impossible to determine the exact time of the eclipse.

the *G* light curve of $[M/H] = -0.81 \pm 0.39$, while Lucchesi et al. (2022) derived a spectroscopic metallicity of $[Fe/H] = -1.95$ and Venn et al. (2020) derived $[Fe/H] = -2.64$. Although the two spectroscopic metallicities disagree, essentially because of the difference in effective temperature (6002 K in Lucchesi et al. 2022 and 5289 K in Venn et al. 2020), they are both at odds with the metallicity from the light curve.

The reason for these discrepancies is not entirely clear to us. The method used in Clementini et al. (2022) employs the empirical calibration found by Nemec et al. (2013), which links the pulsation period and ϕ_{31} parameter of the *G* light curve Fourier decomposition to the metallicity of RR Lyrae. Looking at fig. 11 in Nemec et al. (2013), we note that the outliers are predominantly Blazhko¹² stars. Therefore, it is possible that these stars may be unrecognized Blazhko RR Lyrae. Another possibility could be that, although the RR Lyrae sample used by Nemec et al. (2013) for the calibration is of very good quality, the number of calibrators (41) is not sufficient to provide a precise relation.

5.2 Stars not chemically analysed.

In this section we detail the properties of the non-analysed stars.

5.2.1 *Pristine_002.0937 + 22.6545*

According to Jayasinghe et al. (2018), this star is a detached eclipsing binary of Algol¹³ type with a period of 1.353 5699 d and an amplitude of 0.35 mag. Watson et al. (2006) provide a period of 1.353 57 d, maximum *V* magnitude of 14.74, and minimum *V* magnitude of 15.020. Heinze et al. (2018) classify as ‘dubious’ and provide a period of 0.676 723 d. The *Gaia* DR3 catalogue classifies this star as an eclipsing binary with a *G* amplitude of 0.279 763 mag and a period of 0.672 0462 d. Our *Pristine* photometry combined with *Gaia* photometry and parallax provides 5288./4.35/−1.87. Our spectra are compatible with that of a rapidly rotating K dwarf with a rotational velocity of the order of 70 km s^{-1} . The first spectrum shows a secondary peak, blended with the primary peak, shifted by 72.6 km s^{-1} to the red. The next exposure, taken 40 minutes after the first one, shows a single peak, albeit slightly asymmetric.

5.2.2 *Pristine_024.5944 + 25.4689*

This star is an eclipsing binary of W UMa type according to Jayasinghe et al. (2018) with a period of 0.315 9093 d and an amplitude of 0.48 mag. A similar period (0.315 908 4000 d) is provided by Watson et al. (2006). Also, Chen et al. (2018) classify it as an W UMa type eclipsing binary with a period of 0.31591 d and an amplitude of 0.49 mag. Also, Tian et al. (2020), Heinze et al. (2018), and Marsh et al. (2017) provide an eclipsing binary classification and similar period and amplitude. This star is classified as an eclipsing binary with a period of 0.315 9104 d and an amplitude in the *G* band of 0.519 114 mag in the *Gaia* DR3 catalogue.

¹²The Blazhko effect is a quasi-periodic modulation of the light curve of an RR Lyr star, first observed by Blažko (1907). Kovacs (2016) suggests that 40–50 per cent of the fundamental mode pulsators in the Galaxy display the Blazhko effect. The percentage in the lower metallicity Magellanic Clouds is lower, at most 22 per cent. This effect still lacks an explanation.

¹³The star Algol (β Persei) is the prototype of this class of eclipsing binaries, the luminosity is almost constant except at eclipses, when it sharply drops, with a characteristic almost triangular shape.

Our spectra show very wide lines implying a rotation in excess of 100 km s^{-1} . No $\text{H}\alpha$ absorption is visible, a weak emission is clearly visible. $\text{H}\beta$ is also hardly detectable. The star is an SB2 binary, since the cross-correlation functions show clearly two very wide peaks. The fact that the peaks are so wide make the radial velocity measurement uncertain. The large rotational velocity of both components can be explained by the short orbital period and synchronization of rotational and orbital periods.

5.2.3 *Pristine_029.3591 + 21.3783*

This star is a variable star (Drake et al. 2014; Heinze et al. 2018) and, in fact, an eclipsing binary of W UMa type with a period of 0.35 d (Marsh et al. 2017; Sun et al. 2020). It is classified in the *Gaia* DR3 catalogue as an eclipsing binary with a period of 0.350 0455 d and an amplitude in the *G* band of 0.599 029 mag. According to Sun et al. (2020), the two components have effective temperatures of 5614 and 5637 K, and the masses are 1.35 and $0.34 M_{\odot}$. The primary evolved in order to attain almost equal effective temperatures. The luminosities are 2.21 and $0.68 L_{\odot}$. Our spectra show wide lines, compatible with this kind of stars. The cross-correlation functions with a synthetic template show two very wide peaks, implying the star is an SB2 binary. The two 40 minute exposures, taken one after the other, show displacement of the peaks about 12 km s^{-1} for the primary and 31 km s^{-1} for the secondary. Also in this case, the rapid rotation of both stars can be explained by synchronization of rotational and orbital periods.

5.2.4 *Pristine_034.7189 + 25.9539*

This star is a known eclipsing binary (Drake et al. 2014). According to Marsh et al. (2017), it is a contact binary system with a period of 0.313 6680 d and amplitude of 0.307 mag, the depth of the eclipse is about 0.02 mag, and the effective temperature from the $g - r$ colour is 5792 K. The star is classified as an eclipsing binary in the *Gaia* DR3 catalogue with an amplitude in the *G* band of 0.416 68 mag and a period of 0.313 6690 d.

The spectrum is typical of a G-type dwarf that is rapidly rotating (about 180 km s^{-1}) and shows signs of emission in the Ca II H&K lines. Its metallicity is likely solar. We estimated $T_{\text{eff}} = 5908 \text{ K}$ and $\log g = 4.16$ dex from the $G_{BP} - G_{RP}$ colour and the *Gaia* parallax and *G* magnitude. Such a rapidly rotating G dwarf must be very young, which is consistent with a solar metallicity. The reason why this star has a CaHK photometry that implies a low metallicity is thus clear. The high rotational velocity is probably due to the synchronization of rotational and orbital velocity. The cross-correlation functions show two wide peaks, and the two exposures of about half an hour, taken one after the other, show a change of 7.5 km s^{-1} in the position of the primary peak, and 13.2 km s^{-1} for the secondary. The measurements are however uncertain due to the large width of the cross-correlation peaks.

5.2.5 *Pristine_109.8329 + 41.3782*

This star has no *Gaia* parallax, not even a geometrical distance. According to Heinze et al. (2018) the star is a distant eclipsing binary with a period of 1.053 790 d and a 0.26-mag min–max variation. According to Jayasinghe et al. (2018), it has a period of 1.053 8387 d and an amplitude of 0.21 mag and they classify it as a detached Algol-type system. The two spectra at our disposal show a slight shift in radial velocity over half an hour of the order of 200 m s^{-1} .

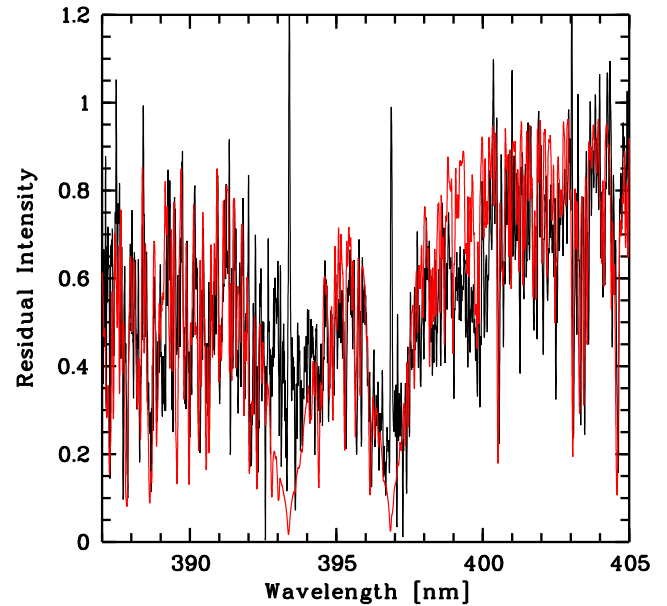


Figure 8. The Ca II H&K lines of *Pristine_148.3782 + 53.0957*, showing a strong emission. For display purposes, the spectrum, sum of the two observed spectra, has been smoothed with a Gaussian with FWHM of 15 km s^{-1} . To guide the eye, the red line is a synthetic spectrum with $T_{\text{eff}}/\log g/[M/H]$ 4527/3.16/−1.5 and a rotational velocity of 26.5 km s^{-1} .

5.2.6 *Pristine_148.3782 + 53.0957*

This star is a known variable (Yao et al. 2015), with amplitude of variation of 0.19 mag and a period of 9.140 132 00 d. However, Heinze et al. (2018) find a period of 27.580 872 d, a factor of three larger, probably an alias of the shorter period, and a much smaller amplitude of variation, 0.09 mag. Tsantaki et al.’s (2022) compilation of radial velocities flags this star as a binary. Tian et al. (2020) report this star in their catalogue of LAMOST radial velocity variables with one spectrum, providing a radial velocity of 9.9 km s^{-1} and another of 45.6 km s^{-1} . The LAMOST effective temperatures, surface gravities, and metallicities are 50 82, 5902; 3.01, 4.36; −0.21, −0.35. *Gaia* DR2 has no variability flag for this star, and *Gaia* EDR3 provides an uncertainty in *G* of 1.8 mmag over 477 observations, of 6.6 mmag in G_{BP} over 53 observations and 5.1 mmag in G_{RP} over 54 observations. *Gaia* DR3 has finally identified the star as a variable. Our derived parameters from the *Gaia* photometry and parallaxes are $T_{\text{eff}} = 4527$ and $\log g = 3.16$. According to *Gaia* DR3 catalogue, this star is an RS CVn rotational variable with an amplitude of variation of 0.14391868 mag in the *G* band. No period is provided. Our spectra do not show any radial velocity variability. The spectrum is characterized by wide lines, which, if interpreted as rotation, imply a $v \sin i$ of 26.5 km s^{-1} . The star is probably slightly metal-poor; in Fig. 8, we show the Ca II H&K lines, characterized by a strong core emission, which is a sign of vigorous chromospheric activity. For display purposes, we plot in Fig. 8 a synthetic spectrum of metallicity −1.5, which is likely a lower limit to the metallicity of this star. The chromospheric activity, testified also by a strong $\text{H}\alpha$ emission, confirms the RS CVn classification for this star.

5.2.7 *Pristine_163.9735 + 13.4823*

According to Sun et al. (2020), this star is an eclipsing binary of W UMa type with a period of 0.325 93 d. The two components have

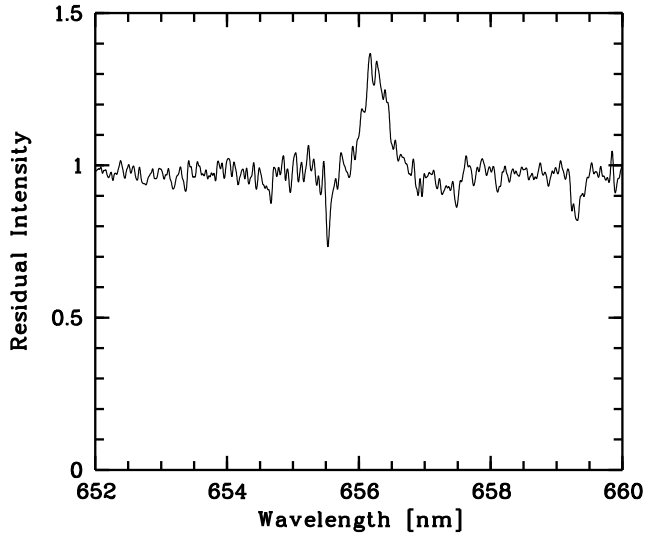


Figure 9. The $H\alpha$ emission in one of the two spectra of Pristine_326.5701 + 19.2445. For display purposes, the spectrum has been smoothed with a Gaussian of 15 km s^{-1} FWHM.

5825 and 6123 K and the masses are 1.24 and $0.3 M_{\odot}$. The star is also classified as an eclipsing binary in the *Gaia* DR3 catalogue, with an amplitude of variation in the *G* band of 0.346752 mag and a period of 0.3259241 d. Although our spectra have an $S/N < 5$ at 550 nm , one can see very wide lines. If the luminosities provided by Sun et al. (2020) are correct ($1.56, 0.26 L_{\odot}$) it seems unlikely that we are seeing the secondary spectrum. In fact the cross-correlation function shows a single very wide peak. The radial velocities measured from both our spectra are consistent within uncertainties.

5.2.8 Pristine_326.5701 + 19.2445

According to Jayasinghe et al. (2018), this star is a spotted star with variability induced by rotation, with a period of 4.5143809 d and an amplitude of 0.2 mag. The period provided by Watson et al. (2006) is 4.5241693000 d and the amplitude 0.191 mag. Chen et al. (2018) classify as an RS CVn star with a period of 4.5241693 d and an amplitude in *g* of 0.214 mag and 0.191 mag in *r*. Heinze et al. (2018) classify it as a Long Period variable and provide a period of 9.011580 d, which looks suspiciously like an alias of the 4.5 -d period provided by the other catalogue. The star is also identified as an RS CVn star in the *Gaia* DR3 catalogue, with an amplitude of variation in the *G* band of 0.236 mag. No period is available. Our spectra show wide lines, implying a rotational velocity around 50 km s^{-1} . There is no evidence of radial velocity variation. There is no measurable flux on Ca II H&K, however, both spectra show an $H\alpha$ emission, shown in Fig. 9, which supports the classification as RS CVn.

5.2.9 Pristine_331.5576 + 27.2164

In Jayasinghe et al. (2018), this star is labelled as an eclipsing binary of type W UMa type with a period of 0.3182321 d and an amplitude of 0.57 mag. *Gaia* DR3 catalogue classifies this star as an eclipsing binary with a *G* amplitude of 0.624458 mag and a period of 0.3182328 d. Our spectra show very wide lines, expected for this kind of star. The star is an SB2 spectroscopic binary. The cross-correlation functions in Fig. 10 show two wide peaks (due to the high rotational velocity), and it is clear that the two peaks move

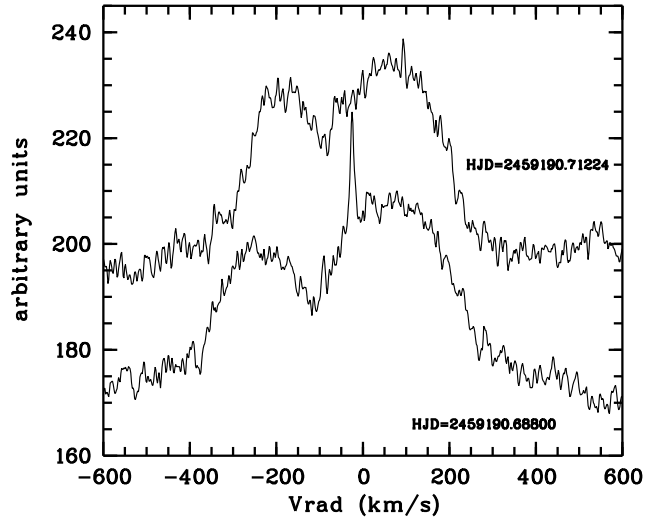


Figure 10. Cross-correlation functions for Pristine_331.5576 + 27.2164. The sharp peak at -24.78 km s^{-1} is due to the solar spectrum, since the observation was taken in twilight.

between the two poses. A very sharp peak appears at -24.78 km s^{-1} . This is the Sun, as this spectrum was taken in twilight, while the next one was already in the astronomical night. Such peaks in the cross-correlation functions of spectra taken at twilight are regularly seen in our spectra. This is due to the fact that the data reduction software does not subtract the solar spectrum, visible in the sky fibre, but just the mean flux. For stars with such wide cross-correlation peaks this is not a problem for the radial velocity measurement.

5.2.10 Pristine_333.2010 + 09.6132

This star is classified as a detached Algol-like eclipsing binary with a period of 9.61327744 d and a magnitude amplitude of 0.32 mag in Jayasinghe et al. (2018). Heinze et al. (2018) classify it as ‘dubious’ and provide a period of 3.199939 . No variability flag is provided in the *Gaia* DR3 catalogue. Our spectra allow us to clearly identify Pristine_333.2010 + 09.6132 as an SB2 system. The cross-correlation function with a synthetic template is clearly double peaked, and there is sizeable difference in the radial velocities between the two exposures, especially for the secondary. There is hardly any signal around the Ca II H&K lines.

5.2.11 Pristine_333.2117 + 20.1267

Numerous sources agree that this star is a variable with a period of around 0.35 d (see e.g. Watson et al. 2006; Drake et al. 2014; Sesar et al. 2017; Chen et al. 2018; Heinze et al. 2018). Watson et al. (2006) and Chen et al. (2018) classify it as an eclipsing binary of W UMa type, while Sesar et al. (2017) classify it as an RR-Lyr variable. The star is classified as an eclipsing binary also in the *Gaia* DR3 catalogue, with a period of 0.3549904 d and a *G* amplitude of 0.593793 mag. The lines in the spectrum are very wide, implying a high rotational velocity, which can be compatible with a W UMa type eclipsing variable, but not with an RR Lyr. The cross-correlation peaks are very wide and there is a considerable radial velocity difference between the two exposures. As for other similar stars, the high rotational velocity of both stars is likely due to synchronization of rotational and orbital periods.

5.2.12 *Pristine_348.1325 + 11.2206*

The star has been identified as an eclipsing binary candidate with a period of 1.75 d by Ferreira Lopes et al. (2015). Both *Gaia* DR2 and DR3 have no variability flag for this star. The LAMOST DR7 catalogue (Luo et al. 2022) provides $T_{\text{eff}} = 5327$ K, $\log g = 3.175$, $[\text{Fe}/\text{H}] = -0.744$, and a radial velocity of 27.58 km s^{-1} . Our spectra show a clear double peak, although the stars are separated by little more than 1 km s^{-1} . The double system of lines can be also appreciated by visual inspection of the spectra. Our radial velocities are very different from that of LAMOST.

6 DISCUSSION AND CONCLUSIONS

It is certainly dismaying that out of the 19 observed stars, only 7 could be subject to our standard analysis, and only two of these were found to be extremely metal-poor. It is however instructive to note how all these stars are indeed extreme, in the sense that there are reasons that make their Ca II H&K photometry ‘weak’. For the stars not analysed, the main reason is the photometric variability. In the second place, SB2 binaries contribute a large fraction of these ‘weak’ Ca II H&K stars (8 out of 19). Fast rotators and active stars also have ‘weak’ Ca II H&K. These reasons explain all the stars not analysed.

Looking at the stars that have been analysed two are photometric variables, *Pristine_328.6116 + 20.3914* and *Pristine_335.8411 + 09.0218*, and so it is not surprising that, although metal-poor, they are not as metal-poor as expected from the Pristine photometry. We consider *Pristine_009.1439 + 15.7850*, *Pristine_159.5695 + 57.1688*, and *Pristine_328.6116 + 20.3914* metal-poor, although the first two stars are not quite as metal-poor as expected. *Pristine_008.1724 + 21.8215* and *Pristine_355.2747 + 26.4757* are significantly more metal-rich than expected, but we have no obvious reason why the metallicity estimate based on Pristine and SDSS photometry failed. This fraction of failures is however to be expected, especially among warm stars. For example, in Bonifacio et al. (2019), we had in the sample nine stars with photometric metallicity below -3.0 ; however, none was this metal poor. The most metal-rich of these stars had $[\text{Fe}/\text{H}] = -0.51$. The most metal-poor star of Bonifacio et al. (2019) sample had metallicity -2.81 , to be compared with a photometric estimate of -2.59 .

It is interesting to consider if some of the variable stars could have been discarded using the information in the *Gaia* DR3 catalogue. Of the 14 photometrically variable stars in our sample, 11 are correctly flagged as VARIABLE in the *Gaia* DR3 catalogue; however, three are not. Fernández-Alvar et al. (2021) suggested using the parameter

$$\sigma_{\text{flux}} = \frac{\sqrt{\text{phot_g_n_obs}}}{\text{phot_g_mean_flux_over_error}} \quad (1)$$

to clean a sample from photometrically variable stars. Since the flux error provided in the *Gaia* catalogue is the error in the mean, i.e. the standard deviation of the flux measurements divided by the square root of the number of measurements, this amounts to using the relative flux error, where the error is simply the standard deviation. If we select only the stars with $\sigma_{\text{flux}} < 0.015$, we still select two eclipsing variables: *Pristine_333.2010 + 09.6132* and *Pristine_348.1325 + 11.2206*. At the same time, *Pristine_328.6116 + 20.3914* and *Pristine_335.8411 + 09.0218* that are variables, but could be analysed, are removed from the sample. Thus, a cut of this kind can be expected to remove about 85 per cent of the photometric variables from the sample. Belokurov et al. (2017)

used essentially the same parameter ($\text{Amp} = \log_{10}(\sigma_{\text{flux}})$) to remove variables. However by considering this parameter for well classified variables in the Magellanic Clouds, they showed that this parameter correlates with the G magnitude and suggested a diagonal line in the G -Amp plane to remove the variable stars. The present sample covers a limited range in G , therefore a simple cut on σ_{flux} is sufficient.

With respect to the expected contaminants we did not find any young, chromospherically active stars. The only two stars with clear chromospheric activity are *Pristine_148.3782 + 53.0957* and *Pristine_326.5701 + 19.2445* that are RS CVn binaries. In this case the chromospheric activity is enhanced by the binary interaction and is not a sign of young age. In fact, the primary is a giant or sub-giant, thus they cannot be very young, because it is necessary for the primary to have evolved. We have no clear explanation for the lack of young stars in our sample. One possibility is that only the most active stars have strong enough emission to affect the Pristine photometry, and these stars are relatively rare. This hypothesis needs to be tested with a larger sample of stars with Pristine photometric metallicity below -3.5 .

The results of this investigation are interesting in the prospect of extensively using Pristine photometry in large spectroscopic surveys, like WEAVE (Jin et al. 2023), to select metal-poor stars. There is an agreement between the WEAVE consortium and the Pristine collaboration, to dedicate a few fibres on every plate for the observation of metal-poor candidates. As a result we expect to observe of the order of 10^5 candidate metal-poor stars in the course of the Survey. Taking the selection efficiency determined in Aguado et al. (2019), we expect about 1×10^4 stars with $[\text{Fe}/\text{H}] \leq -3.0$. Taking the metallicity distribution function of Bonifacio et al. (2021), this implies about 45 stars with $[\text{Fe}/\text{H}] \leq -4.0$, taking into account errors in the MDF, between 0 and 125. According to the SAGA data base (Suda et al. 2008), there are currently 36 known stars with $[\text{Fe}/\text{H}] \leq -4.0$; thus, this can potentially be an increase of a factor of 2. However, to keep these estimates, we must use some filtering on the input catalogues to avoid the stars that appear metal-poor photometrically but are not, like 12 of the targets discussed in this paper. The final lesson to be taken for this sample is that, in order to construct samples with reliable metallicity estimates, one should always remove variable stars, possibly by cross-matching with catalogues that contain variability information. In any case, when extracting the candidates at the extremely low metallicity, one should always expect a few catastrophic mistakes.

ACKNOWLEDGEMENTS

We are grateful to Nadine Manset of CFHT for her help in the interpretation of ESPaDOnS data. We gratefully acknowledge support from the French National Research Agency (ANR) funded project ‘Pristine’ (ANR-18-CE31-0017). P.J. acknowledges financial support from the Swiss National Foundation. Z.Y. acknowledges funding from the Agence Nationale de la Recherche (ANR project ANR-18-CE31-0017). This paper is based on observations obtained with MegaPrime/MegaCam, a joint project of CFHT and CEA/DAPNIA, at the Canada–France–Hawaii Telescope (CFHT), which is operated by the National Research Council (NRC) of Canada, the Institut National des Science de l’Univers of the Centre National de la Recherche Scientifique (CNRS) of France, and the University of Hawaii. The observations at the CFHT were performed with care and respect from the summit of Maunakea, which is a significant cultural and historic

site. This work has made use of data from the European Space Agency (ESA) mission *Gaia* (<https://www.cosmos.esa.int/gaia>), processed by the *Gaia* Data Processing and Analysis Consortium (DPAC; <https://www.cosmos.esa.int/web/gaia/dpac/consortium>). Funding for the DPAC has been provided by national institutions, in particular the institutions participating in the *Gaia* Multilateral Agreement.

DATA AVAILABILITY

The abundance data derived in this paper shall be provided through the Centre de Données astronomiques de Strasbourg. The ESPaDOnS spectra are available through the Canadian Astronomy Data Centre.

REFERENCES

- Abbas M. A., Grebel E. K., Martin N. F., Burgett W. S., Flewelling H., Wainscoat R. J., 2014, *MNRAS*, 441, 1230
- Aguado D. S. et al., 2019, *MNRAS*, 490, 2241
- Aguado D. S. et al., 2022, *A&A*, 668, A86
- Aguado D. S. et al., 2023, *A&A*, 669, L4
- Belokurov V., Erkal D., Deason A. J., Koposov S. E., De Angeli F., Evans D. W., Fraternali F., Mackey D., 2017, *MNRAS*, 466, 4711
- Belokurov V., Erkal D., Evans N. W., Koposov S. E., Deason A. J., 2018, *MNRAS*, 478, 611
- Blažko S., 1907, *Astron. Nachr.*, 175, 325
- Boller T., Freyberg M. J., Trümper J., Haberl F., Voges W., Nandra K., 2016, *A&A*, 588, A103
- Bonifacio P. et al., 2018, *A&A*, 611, A68
- Bonifacio P. et al., 2019, *MNRAS*, 487, 3797
- Bonifacio P. et al., 2021, *A&A*, 651, A79
- Bonifacio P., 1989, Technical Report, NORMA-A Program for the Normalisation of Spectra. Dipartimento di Astronomia dell' Università degli Studi di Trieste
- Boulade O. et al., 2003, in Iye M., Moorwood A. F. M. eds, Proc. SPIE Conf. Ser. Vol. 4841, Instrument Design and Performance for Optical/Infrared Ground-based Telescopes. SPIE, Bellingham, p. 72
- Bovy J., 2015, *ApJS*, 216, 29
- Buder S. et al., 2022, *MNRAS*, 510, 2407
- Caffau E. et al., 2017, *Astron. Nachr.*, 338, 686
- Caffau E. et al., 2020, *MNRAS*, 493, 4677
- Caffau E., Ludwig H. G., Steffen M., Freytag B., Bonifacio P., 2011, *Sol. Phys.*, 268, 255
- Cappellari M., Emsellem E., 2004, *PASP*, 116, 138
- Castelli F., Kurucz R. L., 2003, in Piskunov N., Weiss W. W., Gray D. eds, Proc. IAU Symp. 210, Modelling of Stellar Atmospheres. Kluwer, Dordrecht, p. A20
- Cayrel R. et al., 2004, *A&A*, 416, 1117
- Chen X., Deng L., de Grijs R., Wang S., Feng Y., 2018, *ApJ*, 859, 140
- Chen X., Wang S., Deng L., de Grijs R., Yang M., Tian H., 2020, *ApJS*, 249, 18
- Clementini G. et al., 2022, preprint ([arXiv:2206.06278](https://arxiv.org/abs/2206.06278))
- Doi M. et al., 2010, *AJ*, 139, 1628
- Donati J. F., Catala C., Landstreet J. D., Petit P., 2006, in Casini R., Lites B. W. eds, ASP Conf. Ser. Vol. 358, Solar Polarization 4. Astron. Soc. Pac., San Francisco, p. 362
- Donati J. F., Semel M., Carter B. D., Rees D. E., Collier Cameron A., 1997, *MNRAS*, 291, 658
- Drake A. J. et al., 2013, *ApJ*, 763, 32
- Drake A. J. et al., 2014, *ApJS*, 213, 9
- Fernández-Alvar E. et al., 2021, *MNRAS*, 508, 1509
- Ferreira Lopes C. E., Dékány I., Catelan M., Cross N. J. G., Angeloni R., Leão I. C., De Medeiros J. R., 2015, *A&A*, 573, A100
- Feuillet D. K., Feltzing S., Sahlholdt C. L., Casagrande L., 2020, *MNRAS*, 497, 109
- Franchini M. et al., 2020, *ApJ*, 888, 55
- François P. et al., 2007, *A&A*, 476, 935
- Frebel A., Johnson J. L., Bromm V., 2007, *MNRAS*, 380, L40
- Gaia Collaboration et al., 2016, *A&A*, 595, A1
- Gaia Collaboration et al., 2022, preprint ([arXiv:2208.00211](https://arxiv.org/abs/2208.00211))
- González Hernández J. I. et al., 2008, *A&A*, 480, 233
- Greer P. A., Payne S. G., Norton A. J., Maxted P. F. L., Smalley B., West R. G., Wheatley P. J., Kolb U. C., 2017, *A&A*, 607, A11
- Gustafsson B., Edvardsson B., Eriksson K., Jørgensen U. G., Nordlund Å., Plez B., 2008, *A&A*, 486, 951
- Halbwachs J.-L. et al., 2022, preprint ([arXiv:2206.05726](https://arxiv.org/abs/2206.05726))
- Haywood M., Di Matteo P., Lehnert M. D., Snaith O., Khoperskov S., Gómez A., 2018, *ApJ*, 863, 113
- Heinze A. N. et al., 2018, *AJ*, 156, 241
- Heiter U. et al., 2021, *A&A*, 645, A106
- Helmi A., Babusiaux C., Koppelman H. H., Massari D., Veljanoski J., Brown A. G. A., 2018, *Nature*, 563, 85(GSE)
- Ishigaki M. N., Aoki W., Chiba M., 2013, *ApJ*, 771, 67
- Ishigaki M. N., Chiba M., Aoki W., 2012, *ApJ*, 753, 64
- Jayasinghe T. et al., 2018, *MNRAS*, 477, 3145
- Jin S. et al., 2023, *MNRAS*, tnp..715J
- Kepler S. O. et al., 2016, *MNRAS*, 455, 3413
- Kielty C. L. et al., 2021, *MNRAS*, 506, 1438
- Koposov S. E. et al., 2011, *ApJ*, 736, 146
- Kordopatis G. et al., 2023, *A&A*, 669, A104
- Kovacs G., 2016, Commun. Konkoly Obs. Hungary, 105, 61
- Kučinskas A., Klevas J., Ludwig H. G., Bonifacio P., Steffen M., Caffau E., 2018, *A&A*, 613, A24
- Kurucz R. L., 2005, Mem. Soc. Astron. Ital. Suppl., 8, 14
- Lane J. M. M., Bovy J., Mackereth J. T., 2022, *MNRAS*, 510, 5119
- Lardo C. et al., 2021, *MNRAS*, 508, 3068
- Lindgren L. et al., 2021, *A&A*, 649, A4
- Lodders K., Palme H., Gail H.-P., 2009, *Solar System, Landolt-Börnstein - Group VI Astronomy and Astrophysics*, p. 1616-9573, Springer-Verlag, Berlin
- Lombardo L. et al., 2021, *A&A*, 656, A155
- Lombardo L. et al., 2022, *A&A*, 665, A10
- Lucchesi R. et al., 2022, *MNRAS*, 511, 1004
- Luo A. L. et al., 2022, VizieR Online Data Catalog, p. V/156
- Marsh F. M., Prince T. A., Mahabal A. A., Bellm E. C., Drake A. J., Djorgovski S. G., 2017, *MNRAS*, 465, 4678
- Martínez C. I., Mauas P. J. D., Buccino A. P., 2022, *MNRAS*, 512, 4835
- Mashonkina L., Jablonka P., Pakhomov Y., Sitnova T., North P., 2017, *A&A*, 604, A129
- Masseron T. et al., 2014, *A&A*, 571, A47
- Matsuno T., Aoki W., Suda T., 2019, *ApJ*, 874, L35
- McMillan P. J., 2017, *MNRAS*, 465, 76
- Monty S., Venn K. A., Lane J. M. M., Lokhorst D., Yong D., 2020, *MNRAS*, 497, 1236
- Myeong G. C., Vasiliev E., Iorio G., Evans N. W., Belokurov V., 2019, *MNRAS*, 488, 1235
- Naidu R. P., Conroy C., Bonaca A., Johnson B. D., Ting Y.-S., Caldwell N., Zaritsky D., Cargile P. A., 2020, *ApJ*, 901, 48
- Nemec J. M., Cohen J. G., Ripepi V., Derekas A., Moskalik P., Sesar B., Chadid M., Bruntt H., 2013, *ApJ*, 773, 181
- Press W. H., Teukolsky S. A., Vetterling W. T., Flannery B. P., 1992, Numerical Recipes in FORTRAN. The Art of Scientific Computing, Cambridge University Press
- Randich S., Giampapa M. S., Pallavicini R., 1994, *A&A*, 283, 893
- Rix H.-W., White S. D. M., 1992, *MNRAS*, 254, 389
- Robin A. C., Reylé C., Derrière S., Picaud S., 2003, *A&A*, 409, 523
- Samus' N. N., Kazarovets E. V., Durevich O. V., Kireeva N. N., Pastukhova E. N., 2017, *Astron. Rep.*, 61, 80
- Sbordone L. et al., 2010, *A&A*, 522, A26
- Sbordone L., Caffau E., Bonifacio P., Duffau S., 2014, *A&A*, 564, A109
- Schlafly E. F., Finkbeiner D. P., 2011, *ApJ*, 737, 103
- Sesar B. et al., 2013, *AJ*, 146, 21
- Sesar B. et al., 2017, *AJ*, 153, 204
- Spite F., Spite M., 1982a, *A&A*, 115, 357
- Spite M., Spite F., 1982b, *Nature*, 297, 483

- Starkenburg E. et al., 2017, *MNRAS*, 471, 2587
 Starkenburg E. et al., 2018, *MNRAS*, 481, 3838
 Suda T. et al., 2008, *PASJ*, 60, 1159
 Sun W., Chen X., Deng L., de Grijs R., 2020, *ApJS*, 247, 50
 Tian Z. et al., 2020, *ApJS*, 249, 22
 Tonry J., Davis M., 1979, *AJ*, 84, 1511
 Tsantaki M. et al., 2022, *A&A*, 659, A95
 Venn K. A. et al., 2020, *MNRAS*, 492, 3241
 Venn K. A., Tolstoy E., Kaufer A., Skillman E. D., Clarkson S. M., Smartt S. J., Lennon D. J., Kudritzki R. P., 2003, *AJ*, 126, 1326
 Watson C. L., Henden A. A., Price A., 2006, Soc. Astron. Sci. Annu. Symp., 25, 47
 Yao X. et al., 2015, *AJ*, 150, 107

This paper has been typeset from a $\text{\TeX}/\text{\LaTeX}$ file prepared by the author.